Temperature and Electrical Poling Effects on Ionic Motion in $MAPbI_3$ Photovoltaic Cells

Annalisa Bruno, Daniele Cortecchia, Xin Yu Chin, Kunwu Fu, Pablo P. Boix, Subodh Mhaisalkar, and Cesare Soci*

Despite their excellent power conversion efficiency, $MAPbI_3$ solar cells exhibit strong hysteresis that hinders reliable device operation. Herein it is shown that ionic motion is the dominant mechanism underlying hysteresis of $MAPbI_3$ solar cells by studying the effects of electrical poling in different temperature ranges. Complete suppression of the hysteresis below 170 K is consistent with temperature activated diffusion of I^- anions and/or the motion of the MA^+ cations. Ionic motion has important effect on the overall efficiency of the $MAPbI_3$ solar cells: the initial decrease of the power conversion efficiency while lowering the operating temperature is recovered and even enhanced up to 20% of its original value by applying an electrical poling. The open circuit voltage significantly increases and the current density fully recovers due to the reduction of the electron extraction barrier at the $TiO_2/MAPbI_3$ interface driven by the charge accumulation at the interface. Moreover, beside $TiO_2/MAPbI_3$ interfacial charge transfer, charge transport in TiO_2 strongly affects the photovoltaic performance, as revealed by $MAPbI_3$/ms-TiO_2 field effect transistors. These results establish the basis to develop effective strategies to mitigate operational instability of perovskites solar cells.

1. Introduction

In the last few years, hybrid perovskites have attracted large interest due to their outstanding photovoltaic performances and optoelectronic properties.[1,2] Indeed, the high efficiencies achieved by the lead trihalide perovskites (e.g., $MAPbI_3$) solar cells (SCs) together with low-cost solution processability of the material can lead the evolution of Pb-based hybrid perovskites as a valuable complement technology to silicon-based technology. In few years, SC power conversion efficiency (PCE) has increased from 3.8%[3] in 2009 up to over 20%[4] reaching the world record of 22.1% in early 2016.[1] At the moment device stability and performance reproducibility issues are the main challenges in the development of perovskite-based photovoltaic devices. SCs are affected by significant hysteresis in the current density–voltage (*J–V*) characteristics, and show a strong dependency on the electrical bias history.[5–13] The physical origin of the observed hysteresis has been widely discussed in the recent literature and ascribed to different physical processes: intrinsic $MAPbI_3$ ferroelectricity, presence of defect states at the $MAPbI_3$ surface, voids at the $MAPbI_3/TiO_2$ interface,[14] and ionic motion within the perovskites.[9,14–18] At this stage, the latter is the most accredited phenomenon.[19] Beyond the significant influence on SC *I–V* dependence and hysteresis, ion migration is thought to contribute to many of the unusual phenomena witnessed in hybrid perovskites materials and devices,[13] such as switchable photovoltaic effect,[20] enormous dielectric constant,[21] highly temperature-dependent charge mobilities,[22] photoinduced phase separation,[23] photoinduced self-poling effect,[24] and electrical-field-driven reversible conversion between lead iodide (PbI_2) and $MAPbI_3$.[25] Thus, understanding and controlling the ion-migration mechanisms is critical to improve perovskite-based device performance and stability, both in the dark and under illumination.

In this work, we study $MAPbI_3$-based SCs both in mesoporous (ms-TiO_2) and planar architecture (flat-TiO_2), in the broad temperature range from 298 to 77 K, with the aim of clarifying how charge transfer at $MAPbI_3/TiO_2$ interfaces and charge transport in TiO_2 affect the device efficiency and reliability. We show that hysteresis is highly reduced decreasing the temperature in $MAPbI_3$ SCs and that the initial decrease of the SC efficiency observed by lowering the operation temperature[17,26] can be efficiently recovered, and even increased beyond the initial room temperature value, by applying electrical poling at low temperature. The temperature dependence of the bias poling effect helped in understanding and clarifying the nature of hysteresis in $MAPbI_3$-SCs cells, and the role of $MAPbI_3/TiO_2$ interfaces in charge extraction.

Dr. A. Bruno, D. Cortecchia, Dr. K. Fu, Dr. P. P. Boix, Prof. S. Mhaisalkar
Energy Research Institute @ NTU (ERI@N)
Research Techno Plaza
Nanyang Technological University
50 Nanyang Drive, Singapore 637553, Singapore
E-mail: annalisa@ntu.edu.sg

D. Cortecchia
Interdisciplinary Graduate School
Nanyang Technological University
Singapore 639798, Singapore

X. Y. Chin, Prof. C. Soci
Division of Physics and Applied Physics
School of Physical and Mathematical Sciences
Nanyang Technological University
21 Nanyang Link, Singapore 637371, Singapore

DOI: 10.1002/aenm.201700265

2. Results and Discussions

Hysteresis is the greatest limiting factor of perovskite SCs, and its origin has been widely discussed in last few years.[13,27] It is important to highlight two aspects of this broad scientific debate. On the one hand, "hysteresis free" SCs have been reported when TiO_2 was substituted with different electron transporting layers, such as phenyl-C_{61}-butyric acid methyl ester,[28] while on the other hand large hysteresis was measured in pure $MAPbI_3$ field effect transistors (FETs) that do not include TiO_2.[22] These two observations suggest that hysteresis and device instability are due to a combination of intrinsic $MAPbI_3$ transport characteristics and interfacial properties between $MAPbI_3$ and TiO_2. Consistently, previous works have shown that the Spiro:OMeTAD hole transporting layer does not contribute to the hysteresis.[5,29,30]

$MAPbI_3$ SCs used in this work were prepared in mesoporous (hereafter called SC_m) and planar (hereafter called SC_p) architectures, according to the procedure described in the Experimental Section.

Figure 1a shows the schematic of the mesoporous SC_m used in this work. Figure 1b reports the photocurrent density–voltage curve (J–V) of SC_m at room temperature (298 K), displaying short-circuit current density (J_{sc}) of 20.4 mA cm^{-2}, fill factor (FF) of 61%, and open-circuit voltage (V_{oc}) of 1.03 V, with PCE of 12.8% as measured by a reverse bias scan (Figure 1b). Lower PCE of 7.3% is measured with forward scan direction (red line, Figure 1b), due to the significant current hysteresis. In this case, the FF (38%) is highly reduced, while J_{sc} (19.6 mA cm^{-2}) and V_{oc} (0.99 V) are nearly unaffected. Large current hysteresis is typical of $MAPbI_3$ devices, like SCs and FETs.[22]

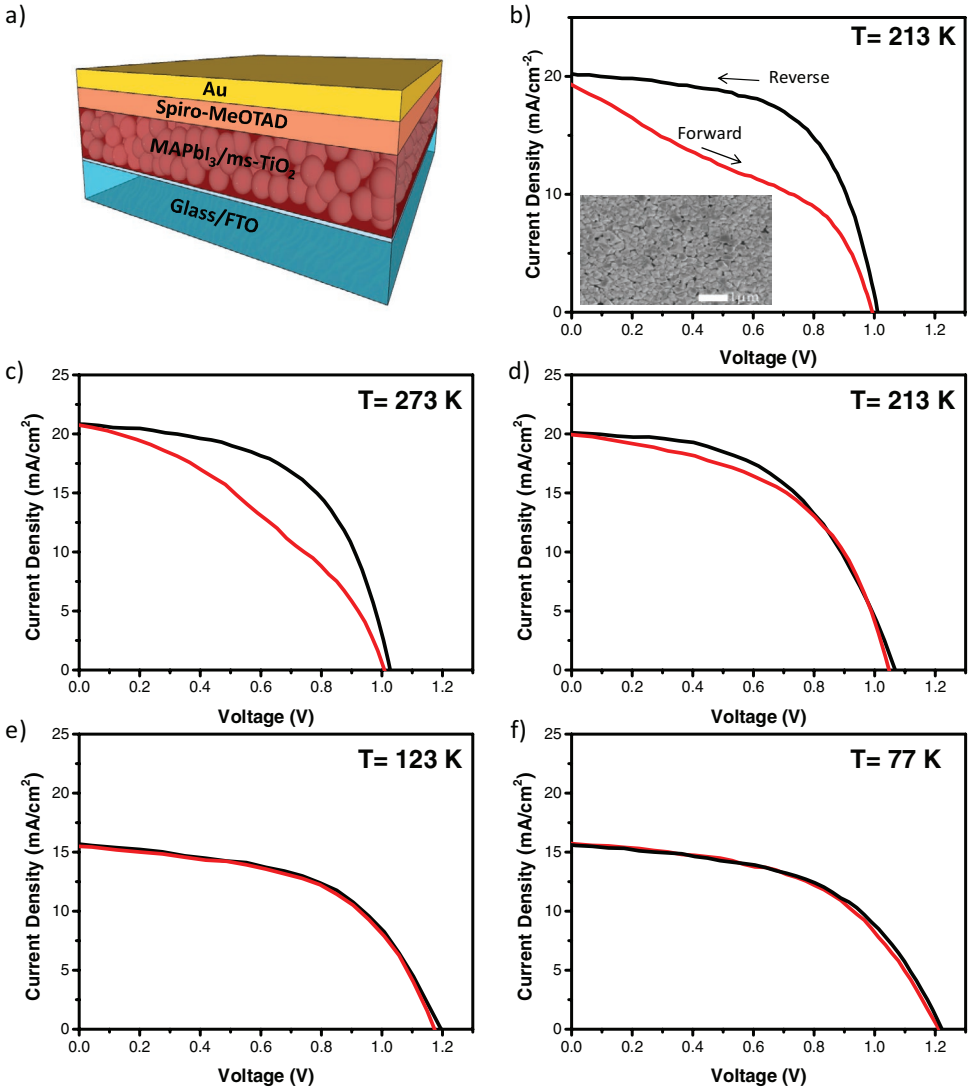

Figure 1. Temperature dependence of mesoporous solar cell characteristics. a) Mesoporous $MAPbI_3$ solar cell (SC_m) device architecture: glass/ITO/FTO/ms-TiO_2/$MAPbI_3$/Spiro/Au. b) J–V curve recorded in forward (red curves) and reverse bias sweeping modes (black curves) at 298 K. Inset: An scanning electron microscopy (SEM) top view image of the $MAPbI_3$ capping layer. c–f) J–V curves at different temperatures, shown in the panels. The voltage scan rate in J–V measurements was kept at 70 mV per step and the waiting time between voltage steps was <0.1 s.

In order to clarify the nature of the photocurrent in SC_m, we measured the *J–V* characteristics at different temperatures, in the range between 298 and 77 K. It has been suggested that ionic motion and vacancy migration may modify the $MAPbI_3$ electronic distribution of states, obstructing charge extraction at selective contacts and affecting SC hysteresis.[31] These phenomena are expected to be strongly temperature dependent.[6,31,32] Some representative *J–V* curves in the temperature range of 298–77 K are reported in Figure 1b–f, showing a rapid reduction of hysteresis while lowering the temperature, with complete suppression of the hysteresis below 170 K. A similar behavior has also been observed in output and transfer characteristics of $MAPbI_3$ FET devices.[22] The hysteresis reduction at low temperature is consistent with ionic motion being the dominant mechanism underlying hysteresis in $MAPbI_3$ SCs, pointing toward the temperature activated diffusion of the MA^+ cations and I^- anions.[33,34] This can be due to a combination of factors. First, at low temperature both I^- anions and MA^+ cations become less mobile and can be stabilized in a specific orientation, reducing the screening effects and increasing stability. Previous observations in the range 170–290 K have shown that the anomalous hysteresis in planar $MAPbI_3$ SC is also strongly temperature dependent, being significantly reduced at 170 K.[17] In the same work, Zou and Holmes[17] have shown that electrical poling at room temperature, followed by cooling under illumination, improved the PCE of a planar $MAPbI_3$ SC from 9% to 14.5%. They also argued that such poling sequence would not be efficient in a mesoporous architecture due to the absence of energy barrier between $MAPbI_3$ and ms-TiO_2.[17] Here we show that low-temperature bias poling allows recovering good SC performance also in $MAPbI_3$/ms-TiO_2 SCs, since it allows overcoming the small energy barrier between TiO_2 and $MAPbI_3$. We also observe that when the SC is brought back to room temperature, hysteresis turns into its original value (Figure S1, Supporting Information), suggesting that the applied bias does not induce a permanent modification to the structure.

The photovoltaic operating parameters, derived from the *J–V* curves in the temperature range from 298 to 77 K, are summarized in **Figure 2**a,b and Figure S2 (Supporting Information). Decreasing the operating temperature and regularly scanning the *J–V* characteristics in the range from 298 to 77 K, the J_{sc} values remain quite stable until 170 K, after which J_{sc} significantly drops down, reaching the minimum value of 15 mA cm^{-2}. At the same time, V_{oc} values remain slightly higher than 1 V until 170 K. Below 170 K, V_{oc} sharply increases reaching 1.22 V at 98 K. To the best of our knowledge, this is the best open circuit voltage reported for pure $MAPbI_3$ SCs. At the same time, the FF does not vary significantly as a function of the temperature (Figure S2, Supporting Information) and as a result the PCE values, shown in Figure 2b, rapidly decrease until 170 K and stabilize around η = 10% below this temperature. Figure 2b (right axis) shows the rapid reduction of hysteresis (≈25% at 298 K) at low temperatures and its nearly complete disappearance (≈1%) below 170 K. These results confirm that the transition from tetragonal to orthorhombic phase has severe effects on transport characteristics of $MAPbI_3$, as discussed in prior literature.[35] Indeed, below 170 K, J_{sc} becomes lower, the hysteresis critically reduces, while the V_{oc} significantly increases. Since $MAPbI_3$ FETs show an increase in mobility at lower temperatures,[22] the decrease of J_{sc} observed here in the orthorhombic phase suggests that in $MAPbI_3$ SCs the current is mostly limited by interfacial effects between the TiO_2 and $MAPbI_3$, rather than by the actual charge transport in $MAPbI_3$. On the other hand, the increase of V_{oc} indicates that at low temperatures charge carrier recombination is reduced,[36] along with the increase of $MAPbI_3$ band gap in the low temperature orthorhombic phase respect to the tetragonal one. *J–V* curve of SC_m at 298 K with PCE of 12.8% is reported in **Figure 3**a (black line), together with the *J–V* curves of the same SC measured at 77 K (green line) after a series of *J–V* measurements at different temperatures between 298 and 77 K. At 77 K the PCE initially dropped down to 10.1%, driven by a decrease of J_{sc} (15.7 mA cm^{-2}) and of the FF (53%). Electrical poling at 77 K allows recovering and even improving the SC performance. Indeed, the *J–V* curve (red line) shows that J_{sc} can be almost completely recovered (with respect to the room temperature values), reaching 19.5 mA cm^{-2}, V_{oc} becomes as high as 1.26 V, and also the FF slightly improves up to 57%, leading to a PCE value as high as 14.2%. This value corresponds to an increase of 20% of the PCE with respect to the value at 298 K.

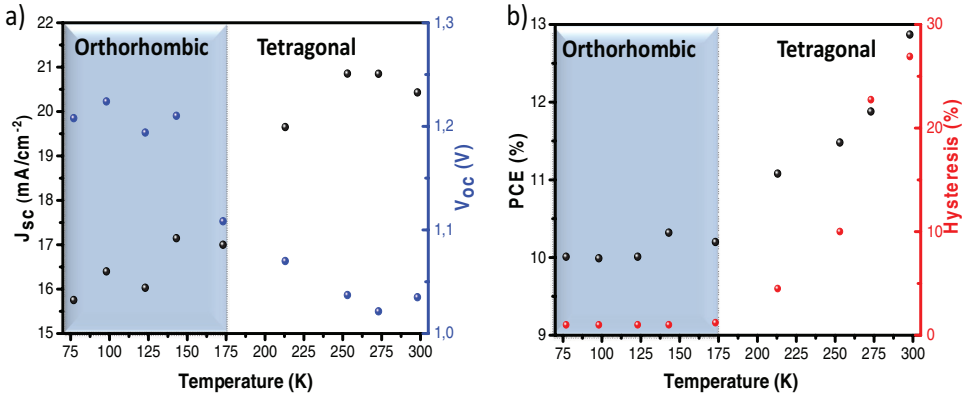

Figure 2. $MAPbI_3$ SC_m operating parameters versus temperature: a) Short circuit current (J_{sc}) and open circuit voltage (V_{oc}); b) power conversion efficiency (PCE) and hysteresis (Hy). Hysteresis was calculated as $\mathrm{Hy}(\%) = 100 * \left(1 - \frac{J_{\text{total Reverse}}}{J_{\text{total Forward}}}\right)$.

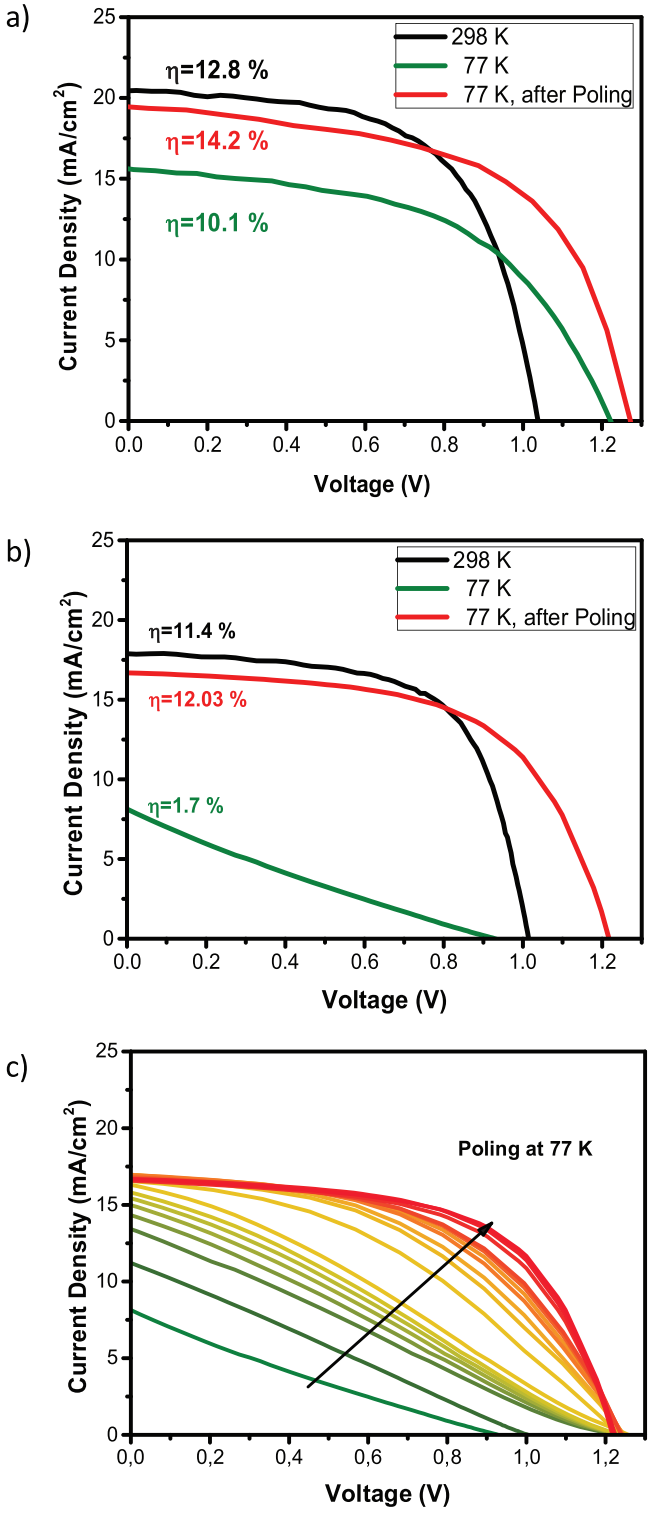

Figure 3. $MAPbI_3$/ms-TiO_2 SCs: a) SC_m *J–V* curves at 298 K (black line), at 77 K (green line) after *J–V* scans were performed regularly at different temperatures intervals in the range 298–77 K, and at 77 K (red line) after the bias poling of 3 V for 180 s has been applied. b) SC_m *J–V* curves at 298 K (black line), at 77 K (green line), and at 77 K (red line) after the poling; c) SC_m *J–V* curves at 77 K applying a 3 V poling for 2 s before each scan.

Figure 3b shows the *J–V* curves of a $MAPbI_3$ SC_m at 298 K (black line), with PCE of 11.4% (J_{sc} = 17.9 mA cm^{-2}, V_{oc} = 1.01 V, FF = 65%), and at 77 K (green line). When the SC is quickly cooled down, the PCE drastically drops to 1.7%, driven by a substantial simultaneous reduction of J_{sc} (8.2 mA cm^{-2}), V_{oc} (0.9 V), and FF (22%). This is a more drastic reduction compared to the one observed when the SC_m is cooled down slowly and *J–V* scans are performed regularly at different temperature intervals. This behavior is indeed similar to what was previously observed in $MAPbI_3$ SCs.[37] Electrical poling of the SC_m at 77 K gradually increases the SC performance, allowing recovering and even improving all the original solar cell parameters. After a few scans, J_{sc}, V_{oc}, and the FF reach values of 16.7 mA, 1.19 V, and 60%, respectively, which corresponds to 12.03% PCE (red line in Figure 2b), higher than the original efficiency (11.4%) of the cell at 298 K. The progressive increase of SC performance after every scan is clear in Figure 3c. The almost complete recovery of the $J_{sc,}$ and the consequent increase of the PCE are compatible with ionic motion under applied electric field. Indeed, ionic migration at the interface can reduce the electron extraction barrier at the $MAPbI_3/TiO_2$, facilitating the electron transfer at the interface. The slow reorientation of MA^+ and the consequent charge accumulation can modify the energy levels and facilitate charge transfers at the interface with TiO_2 after the poling.[13] This behavior is consistent with the slow accumulation of I^- ions at the electrodes. Indeed, it has been demonstrated that I^- ions, which lie at the edge of the PbI_6^{4-} octahedra, are closer to the nearest I^- vacancy with respect to MA^+ and $Pb2^+$ ions, and therefore move faster[38] and they also have a lower activation energy.[31] The slow improvement of the *J–V* characteristic is consistent with the slow accumulation process at the electrodes.[39] These results are an independent proof of how slow accumulation of the I^- at the interface can actually improve charge transfer. This is in agreement with the idea that the organic and inorganic components are strictly linked so that a change in the orientation of the organic cations influences the reorganization of the inorganic ion.[40]

To further investigate the nature of the ionic motion and clarify the role of charge transfer at the interface between TiO_2 and $MaPbI_3$ on the SC_m efficiency, we evaluated the effectiveness of electrical poling in recovering the SC_m performance at different temperatures. The corresponding *J–V* curves are reported in Figure S3 (Supporting Information). If performed before recording a *J–V* scan at 298 K (Figure S3a, Supporting Information), electrical poling slightly improved the SC_m performance both in terms of J_{sc} and V_{oc} and FF, in agreement with similar SCs studies at room temperature.[41] At 263 K, the SC_m performance decreased as expected, and we observed only a slight improvement in the *J–V* curves when poling the SCs. Conversely, despite the reduction of performance upon cooling the SC to 123 K, consecutive electrical poling scans effectively increased J_{sc}, V_{oc}, and FF (Figure S3c, Supporting Information). The same effect was observed at 77 K (Figure 3c). This shows that, at room temperature, the preferential collective orientation of MA^+ cations cannot occur due to high thermal energy, counteracting the action of the applied bias. On the contrary, as the SC is cooled down at 77 K, the reorientation energy of MA^+ cations is significantly lower: this aids the MA^+ reorientation

under applied bias, ultimately enabling charge transfer at the interface with TiO_2. Interestingly, the temperature limit at which this process is energetically favorable coincides with the tetragonal to orthorhombic phase transition temperature (≈170 K). This agrees with the observation that the closer packing of the orthorhombic phase (with respect to the tetragonal phase) can obstruct the rotation of MA^+ cations, leading to a change in the dielectric function.[33]

To better understand the effects of poling on the SC efficiency, the role of $MAPbI_3/TiO_2$ interfaces, and how charge transport in TiO_2 affects the SC performance at different temperatures, we also investigated planar $MAPbI_3$ solar cells. The SC_p architecture is shown in **Figure 4**a, and its preparation procedure is reported in the Experimental Section. SC_p *J–V* curves are shown in Figure 4b, with room temperature PCE of 9.8% (J_{sc} = 18.4 mA cm^{-2}, V_{oc} = 1.04 V, FF = 51%). When the SC_p was directly cooled down to 77 K under illumination, the PCE dropped to 0.65% due to the simultaneous reduction of J_{sc} (6.19 mA cm^{-2}), V_{oc} (0.67 V), and FF (0.14), similar to the case of SC_m. Also in this case, poling continuously increases J_{sc}, V_{oc}, and FF up to 21.4 mA cm^{-2}, 1.2 V, and 39%, respectively, yielding a final PCE of 10.7% (Figure 4c). This value corresponds to a 10% increment compared to the initial PCE value at room temperature.

The temperature dependence of the SC_p performance under the application of electrical poling is reported in Figure S4 (Supporting Information). Very similar to SC_m electrical poling is extremely effective at temperatures below the tetragonal to orthorhombic transition temperature. At 298 K and 173 K, consecutive electrical poling scans do not bear a significant improvement of the SCs performance (Figure S4a,b, Supporting Information). Very differently at 143 and 77 K, when J_{sc}, FF, and V_{oc} are drastically reduced the electrical poling allows us to significantly improve all the SC_p parameters reaching a PCE (11.1% at 77 K) higher with respect to the room temperature one (10.6% at 298 K).

Similar PCE enhancement has been observed under applied bias for both mesoporous and planar architectures. Consistently, poling is effective when applied at temperatures below the tetragonal to orthorhombic phase transition temperature. Despite the much higher interfacial area of the mesoporous with respect to planar architecture, the two SCs undergo a similar increase of J_{sc} with poling: this suggest that J_{sc} increase can be ascribed to a combination of causes, namely, improved charge transfer at the $TiO_2/MAPbI_3$ interface induced by ionic motion in the $MAPbI_3$ and charge transport within TiO_2. The critical role of the $TiO_2/MAPbI_3$ interface has been discussed in previous works reporting different charge separation efficiencies depending also on how the TiO_2 was prepared.[30,42]

To further investigate the charge transfer in $MAPbI_3$ and ms-TiO_2 and the role of the charge transport in TiO_2, we fabricated a "mesoporous FET" ($MAPbI_3$/ms-TiO_2 FET) and measured its output and transfer characteristics as a function of the operating temperature. **Figure 5**a shows the ms-TiO_2 infiltrated with $MAPbI_3$ FET. The temperature evolution of MaPbI3/ms-TiO_2 FET transfer characteristics, from room temperature to 77 K, is provided in Figures S5 and S6 (Supporting Information). The extracted mobility exponentially decreases at low temperatures, as reported in Figure 5b and Figure S7 (Supporting Information), indicating thermally activated charge transport,

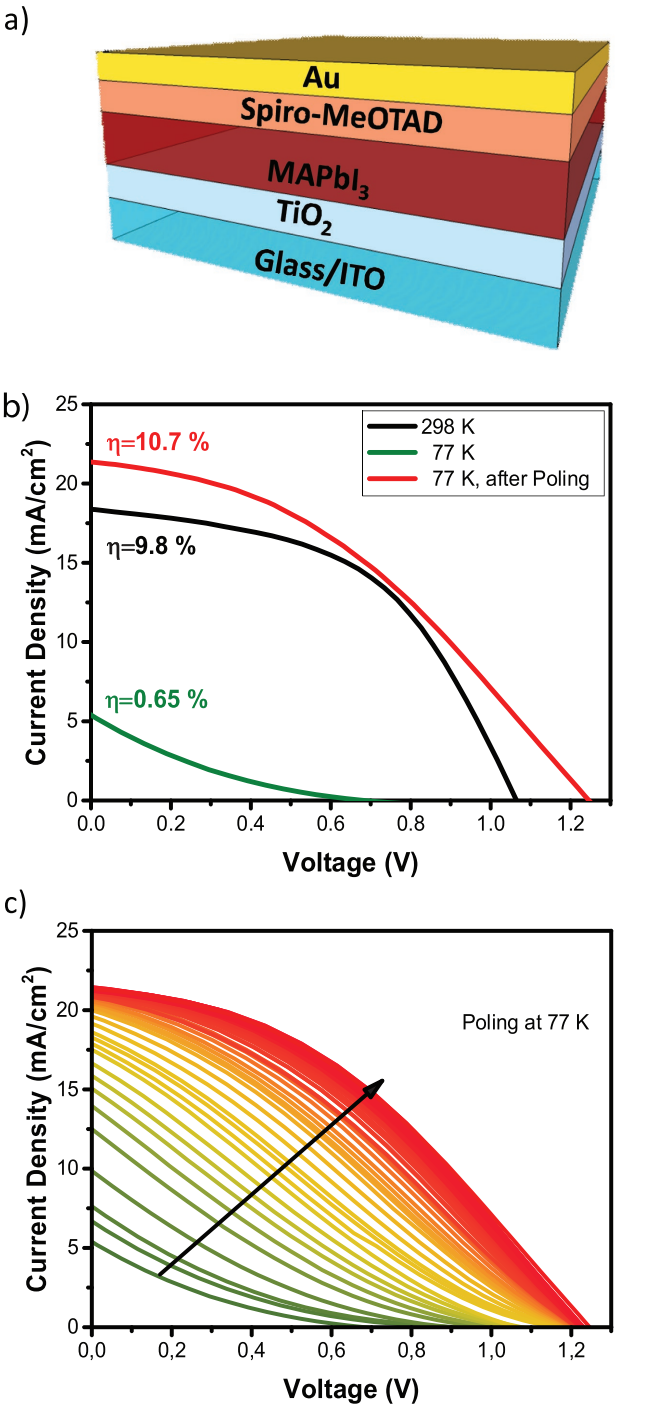

Figure 4. Planar $MAPbI_3$ SC_p. a) Device architecture; b) SC_p *J–V* curves at 298 K (black line), at 77 K (green line), and at 77 K (red line) after the poling; c) SC_p *J–V* curves at 77 K applying a 3 V poling for 2 s before each scan.

in sharp contrast to the inverse temperature-dependent mobility of $MAPbI_3$ FETs.[22] Moreover while plain $MAPbI_3$ FETs show ambipolar behavior,[22] the $MAPbI_3$/ms-TiO_2 FET shows only n-type transport. Both these observations suggest that transport in the mesoporous architecture occurs via two processes: (1) phonon-assisted electron transfer from $MAPbI_3$ to ms-TiO_2

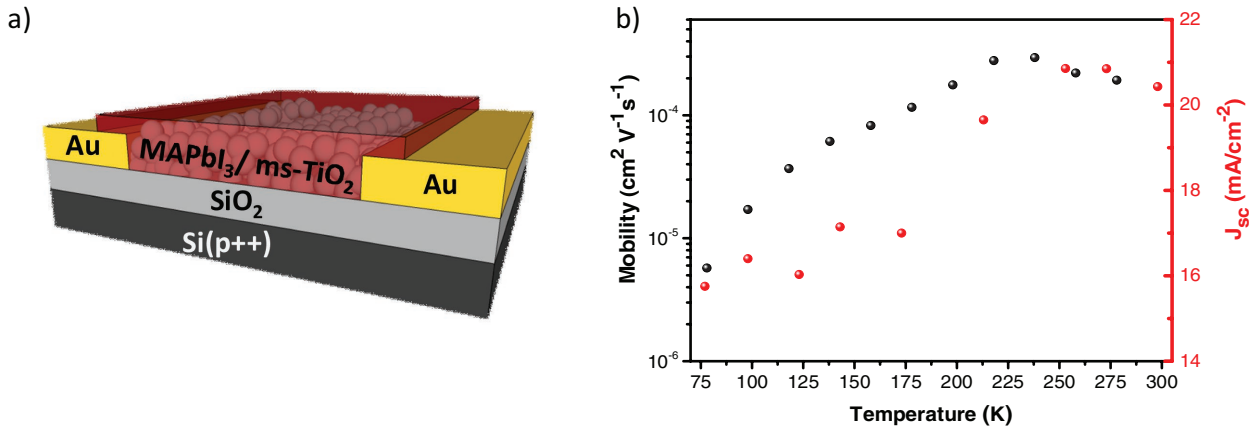

Figure 5. a) Schematic of the bottom-gate, bottom contact $MAPbI_3$/ms-TiO_2 FET used in this work. b) Electron mobility (black full circles) as a function of the temperature and J_{sc} (red full circles) measured in the same temperature range as in the $MAPbI_3$/ms-TiO_2 SC_m.

and (2) electron transport in the TiO_2, acting as n-type semiconductor. We argue that the absence of p-type behavior may be due to the discontinuity of the perovskites at the bottom of the FET channel, which does not form a continuous path for hole transport in the device. These experimental observations suggest that at low temperature charge transfer at $MAPbI_3$/TiO_2 interface and charge transport in the TiO_2 layer are the main limiting factors in this device, rather than the actual charge transport in $MAPbI_3$. The decrease of charge transfer at the interface with TiO_2 as a function of temperature can be ascribed to both the presence of interfacial defects (before the poling is applied)[17,43–45] and the possible increase of the distance between the materials due to the different thermal expansion, which leads to the prominent capacitive effects.[46] The mobility dependence on temperature of the $MAPbI_3$/ms-TiO_2 FET correlates well with the temperature dependence of J_{sc} measured in $MaPbI_3$/ms-TiO_2 SCs (**Figure 6**b).

We have indeed shown that in both mesoporous and flat SCs, the decrease of J_{sc} (together with general SC efficiency) can be compensated by applying a constant electrical poling that facilitates the ionic accumulation at the interface and improves interfacial charge transfer.

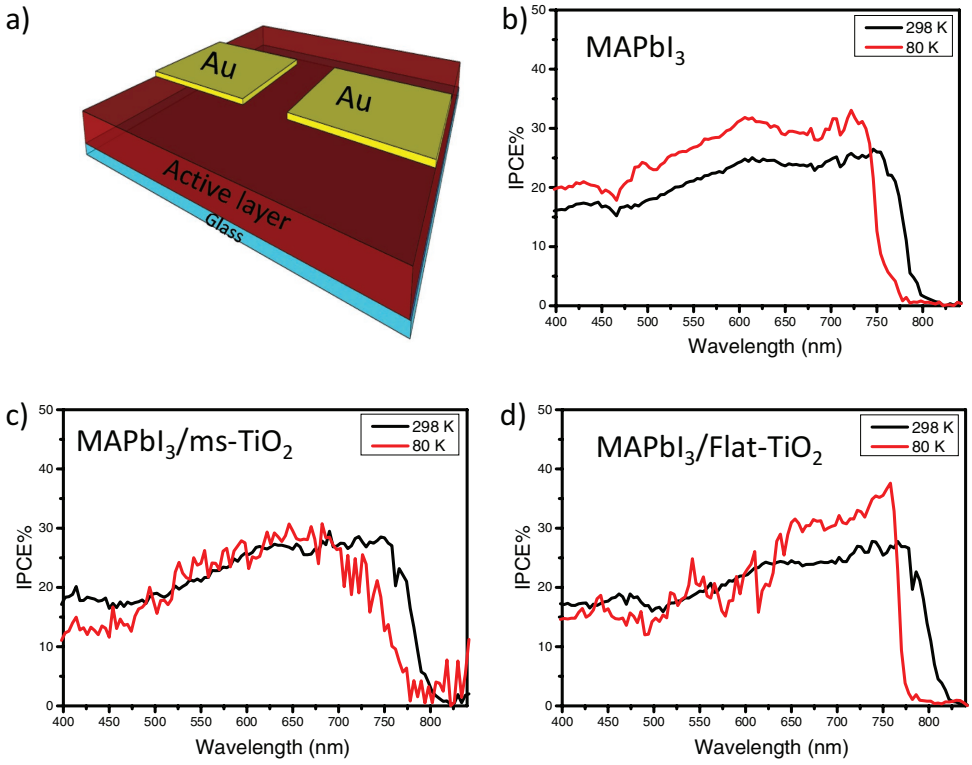

Figure 6. a) Flat device architecture used for IPCE spectra measurements. IPCE spectra at 298 K (black curves) and 77 K (red curves) of: b) $MAPbI_3$, c) $MAPbI_3$/ms-TiO_2, and d) $MAPbI_3$/flat-TiO_2. The device was kept under a constant bias of 2 V during the measurements.

Another proof of the critical role of the $MAPbI_3/TiO_2$ interface on the charge transport properties in SCs is provided by the temperature dependence of the incident photon conversion efficiency (IPCE) in pristine $MAPbI_3$ and $MAPbI_3$/ms-TiO_2 and $MAPbI_3$/flat-TiO_2. The devices were prepared evaporating thin gold contacts (≈100 nm) on top of $MAPbI_3$ and $MAPbI_3$/ms-TiO_2 and $MAPbI_3$/flat-TiO_2 films on glass, in such a configuration to allow the photocurrent measurement on the orthogonal (or lateral) plane (Figure 6a), under a constant 2 V bias. In the pristine $MAPbI_3$ devices (Figure 6b) the total IPCE (and so the total photocurrent) sensibly increases at 77 K compared to the room temperature, in agreement with the higher current density and higher mobility observed in $MAPbI_3$ FETs.[22] In the device with $MAPbI_3$/ms-TiO_2 as active layer (Figure 6c), the total IPCE reduces slightly at 77 K and the spectrum becomes very noisy. These effects may be related to the reduced charge transfer at 77 K, as discussed earlier. Similarly, in $MAPbI_3$/ms-TiO_2 SCs, it is not possible to completely recover the initial room temperature J_{sc}, even if the total PCE of the SC highly increases. Conversely, low temperature poling of $MAPbI_3$/flat-TiO_2 device is much more effective, consistent with the more substantial increase of J_{sc} observed in flat-TiO_2 SC at 77 K upon poling.

A blueshift of the IPCE spectra at low temperature is observable in all three devices. The shift is consistent with the change of structures and absorption proprieties in $MAPbI_3$ passing from the tetragonal to the orthorhombic phase. Indeed $MAPbI_3$ band gap has been previously measured to be ≈1.55 eV at 298 K and ≈1.62 eV at 80 K.[47] The observed blueshift is also consistent with the V_{oc} increase in both types of SCs at 77 K, which contributed to the overall enhancement of the PCE.

3. Conclusions

In the last few years, hybrid organic–inorganic perovskite-based SCs have driven an incredible revolution in the field of photovoltaic, reaching power conversion efficiency values almost comparable to the silicon SC ones. At the moment, the stability issues and the hysteresis in the device *J–V* performances are the main drawback to their implementations in the market. The physical reasons beyond these phenomena are still intensely discussed. Here we have studied the temperature dependence of $MAPbI_3$ mesoporous and planar SC performance under electrical poling in the temperature range from 298 K to 77 K to investigating the nature of the hysteresis and charge transport in $MAPbI_3$ and in TiO_2 and at their interfaces elucidating the fundamental role that ionic motion has in charge transport in perovskites. In $MAPbI_3$ SC_m we show that hysteresis is drastically reduced below the transition temperature (160 K). Moreover, for the first time we show that applying a poling to precondition the SCs, below 170 K, leads to up to an increase of almost 20% of PCE both in mesoporous and in planar SCs. We attribute this behavior to a combination of factors taking place in the SCs, specifically the formation as charge accumulation at the interface due to the ionic motion within the $MAPbI_3$, and the change of charge transfer efficiency at the interface (since the energy barrier between TiO_2 and $MAPbI_3$ is strongly reduced). Our data show that the MA^+ cations at low temperature can be oriented, by electric poling, to facilitate the I^- accumulation at the $TiO_2/MAPbI_3$ interface. Finally, $MAPbI_3$/ms- TiO_2 FET results show that besides the $TiO_2/MAPbI_3$ interfacial charge transfer also the transport in TiO_2 strongly affects the SC performance. We believe these results can establish the basis for strategies to mitigate the operational instability of perovskite SCs by electrical preconditioning.

4. Experimental Section

Material Preparation: Solvents, including chlorobenzene (anhydrous, 99.8%), acetonitrile (anhydrous, 99.8%), and dimethylformamide (anhydrous, 99.8%), were purchased from Sigma-Aldrich. Instead isopropanol was purchased from Fisher Chemical and used as received. PbI_2 (99%) was purchased from Acros. Methylammonium iodide and TiO_2 nanoparticle pastes with 30 nm nanoparticle sizes were purchased from Dyesol Australia (Dyesol 30NRD). 2,2′,7,7′-Tetrakis-(*N*,*N*-di-4-methoxyphenyl-amino)-9,9′-spirobifluorene (Spiro-OMeTAD) was purchased from Merck Chemical (Product ID: SHT-263). All chemicals were used as received without purification.

$MAPbI_3$/ms-TiO_2 SC Fabrication: The detailed process employed for $MAPbI_3$/ms-TiO_2 based solar SC device fabrication is as follows: FTO glass was etched chemically by Zinc powder and diluted HCl acid to designed pattern.[48] The patterned substrate was cleaned with detergent, deionized (DI) water, ethanol, and isopropanol in sequence in ultrasonication bath for 15 min each. A compact layer of TiO_2 was deposited onto the cleaned FTO surface by the spray pyrolysis process using titanium diisopropoxide bis(acetylacetonate) solution (75% in 2-propanol, Sigma-Aldrich) diluted in ethanol (1:9 v/v). After cooling to room temperature, the substrates were treated in a 40×10^{-3} M TiCl 4 solution for 30 min at 70 °C. The $TiCl_4$-treated substrates were sintered at 500 °C for 30 min. 30 nm TiO_2 nanoparticle paste (Dyesol 30NRD) diluted with ethanol (1:3.5 w/w) was spin-coated onto the FTO and sintered at 500 °C for 15 min surface to get mesoporous TiO_2 film. The films were treated with 40×10^{-3} M TiCl 4 $TiCl_4$ solution at 70 °C for 30 min and rinsed and heated at 500 °C again for 30 min. After cooling to room temperature, PbI_2 solution (dissolved in dimethylformamide (DMF)) was spin-coated onto the mesoporous film, which was then heated at 70 °C for 30 min for drying. The films were then immersed into CH_3NH_3I solution in IPA for required duration, after which they were rinsed with isopropyl alcohol and dried by spinning at 4000 rpm for 30 s, followed by annealing at 70 °C for 30 min. The hole transporting material, Spiro-OMeTAD, was dissolved in chlorobenzene at 100 mg mL^{-1}, heating to 70 °C for 30 min for complete dissolvation. Additives such as tert-butylpyridine and lithium bis(trifluoromethylsulfonyl)imide (520 mg mL^{-1} in acetonitrile) were added directly to Spiro-OMeTAD solutions. Co-dopant tris(2-(1H-pyrazol-1-yl)-pyridine)cobalt(III) tris(hexafluorophosphate) (FK102) was predissolved into acetonitrile and added into the hole-transport material solution at 15 mol% concentration. The as-prepared solutions were spin-coated onto the film at 4000 rpm for 30 s. An 80 nm gold cathode layer was deposited by thermal evaporation through a metallic mask to define the cathode area. The cell area is 0.2 cm^2.

$MAPbI_3$/Flat-TiO_2 SC Fabrication: Glass/FTO substrates were cleaned by sonication in Hellmanex detergent, water, acetone, and isopropanol, and finally treated under oxygen plasma for 10 min. To deposit flat TiO_2, 261 mL of titanium (IV) isopropoxide (97%, Sigma-Aldrich) was dissolved in 3.6 mL of isopropanol together with 9 mL of HCl 2M. This precursor solution was spun on the cleaned glass/FTO substrates at 2000 rpm, 60 s, followed by annealing at 500 °C for 45 min. $MAPbI_3$ was deposited on top from a 1.6 M solution in DMF, with addition of dimethylsulfoxide (DMSO) (1:1:1 MAI:PbI_2:DMSO molar ratio). The solution was spun at 4000 rpm, 15 s, with dripping of 300 mL of toluene after 6 s of spinning time. The substrates were annealed at 100 °C for 10 min. A 60×10^{-3} M solution of Spiro-OMeTAD was prepared in chlorobenzene, with addition of bis(trifluoromethane) sulfonimide lithium salt (dissolved in an acetonitrile stock solution, 520 mg mL^{-1})

and 4-tert-butylpyridine, in molar ratios of 50 mol% and 30 mol% with respect to Spiro-OMeTAD, respectively. The resulting solution was spun on the perovskite at 3000 rpm, 60 s. Finally, gold electrodes (75 nm) were thermally evaporated on top of the hole-transporting layer. The same deposition method was used for the fabrication of horizontal devices with structure glass/$MAPbI_3$/Au and glass/flat-TiO_2/$MAPbI_3$/Au used for photocurrent measurements. The cell area is 0.125 cm^2.

SC Characteristic Measurements: J–V measurements were performed using an AM 1.5G solar simulator furnished of a 450 W Xenon lamp (model 81172, Oriel). The power output was adjusted to match AM 1.5G sunlight (100 mW cm^{-2}) by using a reference Si photodiode. *J–V* curves were obtained by applying an external bias to the SC at step of 10 mV and settling time of 0.1 s and measuring the generated photocurrent with a Keithley model 2612A digital source meter. The electrical poling was realized applying a 3 V voltage for 2 s before performing a *J–V* scan in forward mode.

Preparation and Measurements of FET: A heavily p-doped silicon with 500 nm of SiO_2 was used as substrates. The patterning of interdigitated source and drain bottom electrodes (channel length and width of 60 µm and 20 mm, respectively) was obtained by conventional photolithography. 10 nm of Nickel and 50 nm of gold were deposited as source and drain electrodes by thermal evaporation method. 1 g of TiO_2 paste (Dyesol, 30NRD) was diluted with 3.5 g of ethanol and stirred overnight. The resulting suspension was spin-coated at 4000 rpm, 30 s, and the samples annealed at 125 °C, 5 min followed by sintering at 500 °C, 30 min. MAPbI3 was deposited on top from a 1.6 M solution in DFM, with addition of DMSO (1:1:1 MAI:PbI2:DMSO molar ratio). The solution was spun at 4000 rpm, 15 s, with dripping of 300 mL of toluene after 6 s of spinning time. The substrates were annealed at 100 °C for 10 min. The same deposition method was used for the fabrication of horizontal devices with structure glass/ms-TiO_2/MAPbI3/Au used for photocurrent measurements.

FETs were mounted on a temperature-cooling Linkam stage (Linkam FTIR600) with electrical feedthroughs. All FET measurements were performed by using a calibrated Agilent B2902A source-measure unit. FET characteristics were recorded when temperature was stabilized at ±0.5 K of the targeted temperature. Electron mobilities were extracted from the forward sweeping of transfer characteristics obtained at V_{ds} = 100V using the gradual channel approximation in the saturation regime $I_{ds,sat} = \frac{W}{2L}\mu_{sat}C_i\left(V_{gs} - V_{th,sat}\right)^2$. The mobilities were obtained by performing the linear fitting on the $(I_{ds})1/2$ versus V_{gs} plot from data range V_{gs} = 90–100 V. The activation energy (E_{act}) was obtained by fitting the temperature-dependent mobilities with the Arrhenius equation $\mu(T) = \mu_0 \exp(-E_{act}/k_B T)$ in the data range of T = 98–218 K.

IPCE Measurements: The spectral photoresponsivity characteristic was studied with an amplitude modulation technique. The monochromatic light was generated by a combination of Xenon lamp source and JY-IHR 550 monochromator, and modulated by a mechanical chopper at a frequency of 130 Hz. The photocurrent was detected by a lock-in amplifier (SR 830). The optical power density of the incident light was calibrated using a UV-enhanced Si photodiode. All measurements were obtained keeping the device under a constant 2 V bias during the measurement.

Supporting Information

Supporting Information is available from the Wiley Online Library or from the author.

Acknowledgements

This research was supported by the National Research Foundation, Prime Minister's Office, Singapore under its Competitive Research Program (CRP Award No. NRF-CRP14-2014-03). The authors wish to thank Dr. Annamaria Petrozza and Dr. Francesco Maddalena for useful discussions regarding this work.

Conflict of Interest

The authors declare no conflict of interest.

Keywords

electrical poling, hybrid perovskites, ionic screening, *J–V* hysteresis, solar cells

Received: January 27, 2017
Revised: March 3, 2017
Published online:

[1] S. D. Stranks, G. E. Eperon, G. Grancini, C. Menelaou, M. J. P. Alcocer, T. Leijtens, L. M. Herz, A. Petrozza, H. J. Snaith, *Science* **2013**, *342*, 341.
[2] G. Xing, N. Mathews, S. Sun, S. S. Lim, Y. M. Lam, M. Grätzel, S. Mhaisalkar, T. C. Sum, *Science* **2013**, *342*, 344.
[3] A. Kojima, K. Teshima, Y. Shirai, T. Miyasaka, *J. Am. Chem. Soc.* **2009**, *131*, 6050.
[4] a) W. S. Yang, J. H. Noh, N. J. Jeon, Y. C. Kim, S. Ryu, J. Seo, S. I. Seok, *Science* **2015**, *348*, 1234; b) W. Chen, Y. Wu, Y. Yue, J. Liu, W. Zhang, X. Yang, H. Chen, E. Bi, I. Ashraful, M. Grätzel, L. Han, *Science* **2015**, *350*, 944.
[5] H. J. Snaith, A. Abate, J. M. Ball, G. E. Eperon, T. Leijtens, N. K. Noel, S. D. Stranks, J. T. W. Wang, K. Wojciechowski, W. Zhang, *J. Phys. Chem. Lett.* **2014**, *5*, 1511.
[6] L. K. Ono, S. R. Raga, S. Wang, Y. Kato, Y. Qi, *J. Mater. Chem. A* **2015**, *3*, 9074.
[7] L. K. Ono, S. R. Raga, S. Wang, Y. Kato, Y. Qi, *J. Mater. Chem. A* **2015**, *3*, 9074.
[8] W. Tress, N. Marinova, T. Moehl, S. M. Zakeeruddin, M. K. Nazeeruddin, M. Gratzel, *Energy Environ. Sci.* **2015**, *8*, 995.
[9] T. Leijtens, G. E. Eperon, N. K. Noel, S. N. Habisreutinger, A. Petrozza, H. J. Snaith, *Adv. Energy Mater.* **2015**, *5*, 1500963.
[10] M. De Bastiani, G. Dell'Erba, M. Gandini, V. D'Innocenzo, S. Neutzner, A. R. S. Kandada, G. Grancini, M. Binda, M. Prato, J. M. Ball, M. Caironi, A. Petrozza, *Adv. Energy Mater.* **2016**, *6*, 1501453.
[11] S. Wang, Y. Jiang, E. J. Juarez-Perez, L. K. Ono, Y. Qi, *Nat. Energy* **2016**, *2*, 16195.
[12] a) E. L. Unger, E. T. Hoke, C. D. Bailie, W. H. Nguyen, A. R. Bowring, T. Heumuller, M. G. Christoforo, M. D. McGehee, *Energy Environ. Sci.* **2014**, *7*, 3690; b) D. A. Egger, A. M. Rappe, L. Kronik, *Acc. Chem. Res.* **2016**, *49*, 573; c) K. Domanski, B. Roose, T. Matsui, M. Saliba, S.-H. Turren-Cruz, J.-P. Correa-Baena, C. R. Carmona, G. Richardson, J. M. Foster, F. De Angelis, J. M. Ball, A. Petrozza, N. Mine, M. K. Nazeeruddin, W. Tress, M. Gratzel, U. Steiner, A. Hagfeldt, A. Abate, *Energy Environ. Sci.* **2017**, *9*, 1989.
[13] Y. Yuan, J. Huang, *Acc. Chem. Res.* **2016**, *49*, 286.
[14] A. K. Jena, H.-W. Chen, A. Kogo, Y. Sanehira, M. Ikegami, T. Miyasaka, *ACS Appl. Mater. Interfaces* **2015**, *7*, 9817.
[15] a) J. M. Frost, K. T. Butler, A. Walsh, *APL Mater.* **2014**, *2*, 081506; b) G. Niu, X. Guo, L. Wang, *J. Mater. Chem. A* **2015**, *3*, 8970.
[16] N. E. Chart, http://www.nrel.gov/ncpv/images/efficiency_chart.jpg (accessed December: 2016).
[17] Y. Zou, R. J. Holmes, *Adv. Energy Mater.* **2016**, *6*, 1501994.

[18] Y. Bi, E. M. Hutter, Y. Fang, Q. Dong, J. Huang, T. J. Savenije, *J. Phys. Chem. Lett.* **2016**, *7*, 923.
[19] a) C. Eames, J. M. Frost, P. R. F. Barnes, B. C. O'Regan, A. Walsh, M. S. Islam, *Nat. Commun.* **2015**, *6*, 7497; b) J. Mizusaki, K. Arai, K. Fueki, *Solid State Ionics* **1983**, *11*, 203.
[20] Z. Xiao, Y. Yuan, Y. Shao, Q. Wang, Q. Dong, C. Bi, P. Sharma, A. Gruverman, J. Huang, *Nat. Mater.* **2015**, *14*, 193.
[21] E. J. Juarez-Perez, R. S. Sanchez, L. Badia, G. Garcia-Belmonte, Y. S. Kang, I. Mora-Sero, J. Bisquert, *J. Phys. Chem. Lett.* **2014**, *5*, 2390.
[22] X. Y. Chin, D. Cortecchia, J. Yin, A. Bruno, C. Soci, *Nat. Commun.* **2015**, *6*, 7383.
[23] D. W. deQuilettes, W. Zhang, V. M. Burlakov, D. J. Graham, T. Leijtens, A. Osherov, V. Bulovic, H. J. Snaith, D. S. Ginger, S. D. Stranks, *Nat. Commun.* **2016**, *7*, 11683.
[24] Y. Deng, Z. Xiao, J. Huang, *Adv. Energy Mater.* **2015**, *5*, 1500721.
[25] Y. Yuan, Q. Wang, Y. Shao, H. Lu, T. Li, A. Gruverman, J. Huang, *Advanced Energy Materials* **2016**, *6*, 1501803.
[26] H. Zhang, X. Qiao, Y. Shen, T. Moehl, S. M. Zakeeruddin, M. Gratzel, M. Wang, *J. Mater. Chem. A* **2015**, *3*, 11762.
[27] B. Chen, M. Yang, S. Priya, K. Zhu, *J. Phys. Chem. Lett.* **2016**, *7*, 905.
[28] a) H. Yoon, S. M. Kang, J.-K. Lee, M. Choi, *Energy Environ. Sci.* **2016**, *9*, 2262; b) J.-P. Correa-Baena, A. Abate, M. Saliba, W. Tress, T. Jesper Jacobsson, M. Gratzel, A. Hagfeldt, *Energy Environ. Sci.* **2017**, *10*, 710.
[29] a) W. Kong, Z. Ye, Z. Qi, B. Zhang, M. Wang, A. Rahimi-Iman, H. Wu, *Phys. Chem. Chem. Phys.* **2015**, *17*, 16405; b) G. Xing, B. Wu, S. Chen, J. Chua, N. Yantara, S. Mhaisalkar, N. Mathews, T. C. Sum, *Small* **2015**, *11*, 3606.
[30] R. Gottesman, E. Haltzi, L. Gouda, S. Tirosh, Y. Bouhadana, A. Zaban, E. Mosconi, F. De Angelis, *J. Phys. Chem. Lett.* **2014**, *5*, 2662.
[31] J. M. Azpiroz, E. Mosconi, J. Bisquert, F. De Angelis, *Energy Environ. Sci.* **2015**, *8*, 2118.
[32] Y. Yuan, J. Chae, Y. Shao, Q. Wang, Z. Xiao, A. Centrone, J. Huang, *Adv. Energy Mater.* **2015**, *5*, 1500615.
[33] G. Richardson, S. E. J. O'Kane, R. G. Niemann, T. A. Peltola, J. M. Foster, P. J. Cameron, A. B. Walker, *Energy Environ. Sci.* **2016**, *9*, 1476.
[34] G. Xing, N. Mathews, S. S. Lim, N. Yantara, X. Liu, D. Sabba, M. Grätzel, S. Mhaisalkar, T. C. Sum, *Nat. Mater.* **2014**, *13*, 476.
[35] Y. Zhang, M. Liu, G. E. Eperon, T. C. Leijtens, D. McMeekin, M. Saliba, W. Zhang, M. de Bastiani, A. Petrozza, L. M. Herz, M. B. Johnston, H. Lin, H. J. Snaith, *Mater. Horiz.* **2015**, *2*, 315.
[36] C. Tao, J. Van Der Velden, L. Cabau, N. F. Montcada, S. Neutzner, A. R. Srimath Kandada, S. Marras, L. Brambilla, M. Tommasini, W. Xu, R. Sorrentino, A. Perinot, M. Caironi, C. Bertarelli, E. Palomares, A. Petrozza, *Adv. Mater.* **2017**, *29*, 1604493.
[37] H. Zhang, X. Qiao, Y. Shen, T. Moehl, S. M. Zakeeruddin, M. Gratzel, M. Wang, *J. Mater. Chem. A* **2015**, *3*, 11762.
[38] C. Eames, J. M. Frost, P. R. F. Barnes, B. C. O'Regan, A. Walsh, M. S. Islam, *Nat. Commun.* **2015**, *6*, 7497.
[39] B. Wu, K. Fu, N. Yantara, G. Xing, S. Sun, T. C. Sum, N. Mathews, *Adv. Energy Mater.* **2015**, *5*, 1500829.
[40] a) E. Mosconi, F. De Angelis, *ACS Energy Lett.* **2016**, *1*, 182; b) C. Quarti, E. Mosconi, F. De Angelis, *Chem. Mater.* **2014**, *26*, 6557.
[41] J. A. Christians, J. S. Manser, P. V. Kamat, *J. Phys. Chem. Lett.* **2015**, *6*, 852.
[42] a) M. D. Birowosuto, D. Cortecchia, W. Drozdowski, K. Brylew, W. Lachmanski, A. Bruno, C. Soci, *Sci. Rep.* **2016**, *6*, 37254; b) Q. Chen, N. De Marco, Y. Yang, T.-B. Song, C.-C. Chen, H. Zhao, Z. Hong, H. Zhou, Y. Yang, *Nano Today* **2015**, *10*, 355.
[43] Q. Wang, Y. Shao, H. Xie, L. Lyu, X. Liu, Y. Gao, J. Huang, *Appl. Phys. Lett.* **2014**, *105*, 163508.
[44] V. Roiati, E. Mosconi, A. Listorti, S. Colella, G. Gigli, F. De Angelis, *Nano Lett.* **2014**, *14*, 2168.
[45] B. C. O'Regan, P. R. F. Barnes, X. Li, C. Law, E. Palomares, J. M. Marin-Beloqui, *J. Am. Chem. Soc.* **2015**, *137*, 5087.
[46] a) L. Cojocaru, S. Uchida, Y. Sanehira, V. Gonzalez-Pedro, J. Bisquert, J. Nakazaki, T. Kubo, H. Segawa, *Chem. Lett.* **2015**, *44*, 1557; b) B. Chen, M. Yang, X. Zheng, C. Wu, W. Li, Y. Yan, J. Bisquert, G. Garcia-Belmonte, K. Zhu, S. Priya, *J. Phys. Chem. Lett.* **2015**, *6*, 4693.
[47] V. D'Innocenzo, G. Grancini, M. J. Alcocer, A. R. Kandada, S. D. Stranks, M. M. Lee, G. Lanzani, H. J. Snaith, A. Petrozza, *Nat. Commun.* **2014**, *5*, 3586.
[48] A. Krishna, D. Sabba, J. Yin, A. Bruno, P. P. Boix, Y. Gao, H. A. Dewi, G. G. Gurzadyan, C. Soci, S. G. Mhaisalkar, A. C. Grimsdale, *Chem.—Eur. J.* **2015**, *21*, 15113.

